

LETTER TO THE EDITOR

# First VLBI detection of Fornax A

G. F. Paraschos<sup>1</sup>, M. Wielgus<sup>1,2</sup>, P. Benke<sup>1</sup>, V. Mpisketzis<sup>3,4</sup>, F. Rösch<sup>5</sup>, K. Dasyra<sup>3</sup>, E. Ros<sup>1</sup>,  
M. Kadler<sup>5</sup>, R. Ojha<sup>6</sup>, P. G. Edwards<sup>7</sup>, L. Hyland<sup>8</sup>, J. F. H. Quick<sup>9</sup>, S. Weston<sup>10</sup>

<sup>1</sup>Max-Planck-Institut für Radioastronomie, Auf dem Hügel 69, D-53121 Bonn, Germany  
e-mail: gfparaschos@mpi-fr-bonn.mpg.de

<sup>2</sup>Institute of Physics, Silesian University in Opava, Bezručovo nám. 13, CZ-746 01 Opava, Czech Republic

<sup>3</sup>Department of Physics, National and Kapodistrian University of Athens, Panepistimiopolis, 15783 Zografos, Greece

<sup>4</sup>Institut für Theoretische Physik, Goethe Universität Frankfurt, Max-von-Laue-Str.1, 60438 Frankfurt am Main, Germany

<sup>5</sup>Julius Maximilians University Würzburg, Faculty of Physics and Astronomy, Institute for Theoretical Physics and Astrophysics, Chair of Astronomy, Emil-Fischer-Str. 31, 97074 Würzburg, Germany

<sup>6</sup>NASA HQ, 300 E St SW, Washington, DC 20546-0002, USA

<sup>7</sup>CSIRO Space and Astronomy, PO Box 76, Epping, NSW1710, Australia

<sup>8</sup>School of Natural Sciences, University of Tasmania, Private Bag 37, Hobart, Tasmania 7001, Australia

<sup>9</sup>Hartebeesthoek Radio Astronomy Observatory, PO Box 443, 1740 Krugersdorp, South Africa

<sup>10</sup>Space Operations New Zealand Ltd, 62 Deveron Street, Invercargill 984, New Zealand

Received -; accepted -

## ABSTRACT

Radio galaxies harbouring jetted active galactic nuclei are a frequent target of very-long-baseline interferometry (VLBI) because they play an essential role in exploring how jets form and propagate. Hence, only few have not been detected with VLBI yet; Fornax A is one of the most famous examples. Here we present the first detection of the compact core region of Fornax A with VLBI. At 8.4 GHz the faint core is consistent with an unresolved point source. We constrained its flux density to be  $S_0 = 47.5 - 62.3$  mJy and its diameter to be  $D_0^{\text{min}} \leq 70$   $\mu\text{s}$ . The high values of the measured brightness temperature ( $T_B \gtrsim 10^{11}$  K) imply that the observed radiation is of non-thermal origin, likely associated with the synchrotron emission from the active galactic nucleus. We also investigated the possibility of a second radio source being present within the field of view. Adding a second Gaussian component to the geometrical model-fit does not significantly improve the quality of the fit and we, therefore, conclude that our detection corresponds to the compact core of Fornax A. Analysis of the non-trivial closure phases provides evidence for the detection of more extended flux density, on the angular scale of  $\sim 4000$   $\mu\text{s}$ . Finally, the fractional circular polarisation of the core is consistent with zero, with a conservative upper limit being  $m_{\text{circ}} \leq 4\%$ .

**Key words.** Galaxies: jets – Galaxies: active – Galaxies: individual: Fornax A (NGC 1316) – Techniques: interferometric – Techniques: high angular resolution

## 1. Introduction

Relativistic astrophysical jets emanating from the centres of galaxies are a telltale sign of highly energetic activity connected to the central supermassive black hole (SMBH) that they harbour. Specifically, radio galaxies with an active galactic nucleus (AGN) are a ubiquitous target of jet studies, since they are generally nearby and therefore provide more insights into jet formation and launching. At larger scales, jet interactions with the ambient medium can give clues about AGN feedback, star formation, and galactic evolution (e.g. Fabian et al. 2000; García-Burillo et al. 2014; Fotopoulou et al. 2019; Dasyra et al. 2022). On the other hand, at smaller scales, the ultimate vicinity of SMBHs can be explored using very-long-baseline interferometry (VLBI), with which the shrouding medium around them can be peered through. Such studies have been carried out, for example, for M 87 (EHTC et al. 2019; Lu et al. 2023), Sgr A\* (EHTC et al. 2022), Cygnus A (Boccardi et al. 2016), 3C 84 (Nagai et al. 2014; Paraschos et al. 2021, 2022), NGC 1052 (Baczko et al. 2016), and Centaurus A (Müller et al. 2011, 2014; Kim et al. 2018; Janssen et al. 2021) among others.

Fornax A (NGC 1316, J0322-3712) is another such radio galaxy whose radio emission is very prominent, providing clues about its central engine. It is located in the Fornax cluster and is one of the nearest ( $D_L = 18.8$  Mpc; Hatt et al. 2018) and brightest (e.g. Cantiello et al. 2013) radio galaxies, harbouring a SMBH of  $\sim 1.3 \times 10^8 M_\odot$  (Nowak et al. 2008). This system is thought to be the result of more than one merger event (Schweizer 1980; Mackie & Fabbiano 1998; Lanz et al. 2010; Richtler et al. 2012a,b). Consequently, it has been the target of numerous studies, covering a wide frequency spectrum (see Stanley & Slee 1950; Schweizer 1980; Geldzahler & Fomalont 1984; Horellou et al. 2001; Lanz et al. 2010; Richtler et al. 2012a; Maccagni et al. 2020, among others). The most prominent morphological characteristic of Fornax A are two extended radio jets (the centres of the two lobes are  $\sim 30$  arcmin apart, with total edge-to-edge size  $\leq 50$  arcmin; see e.g. Ekers et al. 1983) emanating from the central AGN, encased in dense interstellar medium. Their larger scale physical characteristic have been studied with radio and X-ray observations, revealing variability in the orientation of the inner jets (Geldzahler & Fomalont 1984) and associated X-ray cavities (Lanz et al. 2010). Most recently, MeerKat data showed that the radio lobes of Fornax A

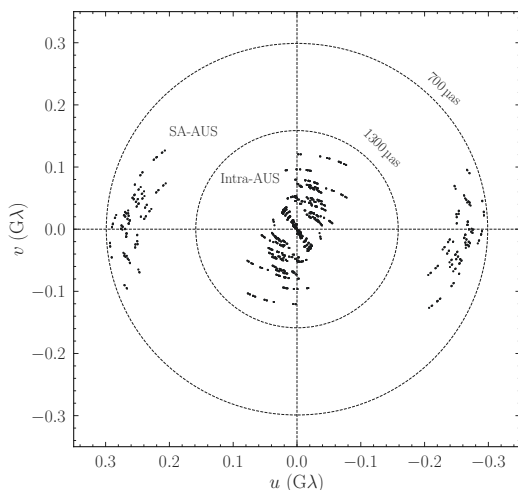


Fig. 1: Illustration of the TANAMI  $(u, v)$ -coverage of the target source Fornax A. Two point clouds can be identified in the  $(u, v)$ -coverage, corresponding to the shorter distance Intra-Australian/New Zealand baselines and to the ones between Australia/New Zealand and South Africa. The outer dashed circle corresponds to a  $(u, v)$ -radius of 700 micro-arcseconds ( $\mu\text{as}$ ) and the inner one to 1300  $\mu\text{as}$ .

have a double shell morphology and that its core is rapidly flickering (Maccagni et al. 2020). The complexity of its structure has been connected to past merger events (Lanz et al. 2010; Richtler et al. 2012a,b), possibly associated with its numerous occurrences of intermittent radio activity (Maccagni et al. 2020).

Nevertheless, Fornax A has not been detected with VLBI thus far (Slee et al. 1990; Fomalont et al. 2000; Angioni et al. 2019). This is because VLBI monitoring of the southern sky is limited and this source exhibits a faint nuclear region. With our exploratory observations, we aimed to study the core region of Fornax A, peering as far as possible into the vicinity of the central engine. Here we report the first VLBI detection of this compact region of Fornax A, with which we were able to constrain the size and structure of its core. This work is structured as follows: In Sect. 2 we present the observational setup, our data analysis methodology, and our results. In Sect. 3 we discuss constraints of the core structure and polarisation and in Sect. 4 we conclude with a summary of this work.

## 2. Observations, data analysis, and results

Fornax A was observed in X-band (8.4 GHz) on February 11 2023 for a total of one hour as a test source, as part of the VLBI monitoring program Tracking Active Galactic Nuclei with Austral Milliarsecond Interferometry (TANAMI; see Ojha et al. 2010). The participating antennas ATCA (AT;  $5 \times 22$  m), Ceduna (CD; 30 m), Hobart (HO; 26 m), Katherine (KE; 12 m), Mopra (MP; 22 m), Parkes (PA; 64 m), DSS36 (TD; 34 m), and DSS43 (TI; 70 m) in Australia, Warkworth (WW; 12 m) in New Zealand, and Hartebeesthoek (HH; 26 m) in South Africa. Further details about them can be found in Benke et al. (2024). In Fig. 1 we display the  $(u, v)$ -coverage corresponding to observations of Fornax A with the TANAMI array.

We conducted the data calibration with the software package AIPS (Greisen 2003). The standard VLBI procedure was followed (described in more detail in Benke et al. 2024), in which digital sampling and parallactic angle corrections were

applied to the data and fringe fitting and amplitude calibration were performed. A fringe fitting signal-to-noise ratio ( $S/N$ ) detection threshold of  $5\sigma$  was imposed. Phase-referenced calibration was also performed, however, this approach did not yield an increase in the number of detections and the final data products did not exhibit any discernible difference. Finally, the data were averaged in frequency (to output a single channel per sub-band) and coherently in time (into ninety second bins), and then written out for image reconstruction. The final  $S/N$  in the range of  $S/N \sim 5 - 30$  provided a solid basis for our subsequent analysis.

The challenges of the analysis of the Fornax A data set are caused by the sparse  $(u, v)$ -coverage with a large gap between approximately 0.1 and 0.2  $G\lambda$  (see Fig. 1) related to the geographic spread of the antennas that comprise TANAMI and uncertainties of the amplitude gain calibration in the absence of strongly constraining interferometric closure information. To leverage relatively high  $S/N$  and to mitigate potential spurious instrumental effects or artefacts in our data, we employed two methods for the source morphology reconstruction. Our first approach was to use the CLEAN algorithm within the `dmfmap` software package (Shepherd et al. 1994). The image is shown in the left panel of Fig. 2; the structure is consistent with a compact point source. As a second step we modelled the flux density with a circular Gaussian component. The best fit parameters for flux density ( $S_0^{\text{clean}}$ ) and diameter ( $D_0^{\text{clean}}$ ) were:  $S_0^{\text{clean}} = 62.3 \pm 6.2$  mJy and  $D_0^{\text{clean}} = 96.0$   $\mu\text{as}$ .

Our second approach was to use geometrical modelling within the `eht-imaging` framework (Chael et al. 2016; Roelofs et al. 2023). The advantage of this forward-modelling technique lies in the fact that best-fit solutions are leveraged from the data without the necessity of convolving the solution afterwards with the point-spread function. Thus, more fine structure can be recovered and information can be extracted even from sparse datasets (see e.g. Paraschos et al. 2024), without performing full-fledged imaging. The right panel of Fig. 2 presents our best-fit model to the visibility amplitudes and closure phases as a function of the  $(u, v)$ -distance. In this case the input model used was an elliptical Gaussian component. However, the best fit was achieved when the major axis of the ellipse equalled the minor one, resulting again in a circular Gaussian component, characterised by a flux density of  $S_0^{\text{ehtim}} = 47.5 \pm 4.8$  mJy and a diameter of  $D_0^{\text{ehtim}} = 10.0$   $\mu\text{as}$ . We note here that  $D_0^{\text{ehtim}}$  corresponds to the lower limit of the allowed parameter extent.

Using the formalism described in Lobanov (2005), we then calculated the minimum resolvable scale of our observations, which corresponds to  $D_{\text{lim}} = 70$   $\mu\text{as}$ . Since from our two approaches we constrained diameter of the compact source to a lower value on average, this implies that the compact source is consistent with an unresolved point source ( $D_0^{\text{min}} \leq 70$   $\mu\text{as}$ ). The bottom panel of Fig. 2 showcases the fitted data and the geometrical model used. The measurements at longer baselines correspond to robust detections, with an  $S/N$  of  $\geq 5$ , indicative of a very compact structure.

We also constrained the flux density of the source's core to be  $S_0 = 47.5 - 62.3$  mJy. In order to transform this into the observed brightness temperature  $T_B$ , we used the formula:

$$T_B = 1.22 \times 10^{15} \left( \frac{S}{\text{mJy}} \right) \left( \frac{\nu}{\text{GHz}} \right)^{-2} \left( \frac{\phi}{\mu\text{as}} \right)^{-2}, \quad (1)$$

where  $\nu$  is the observing frequency and  $\phi$  is the source size (or a corresponding upper limit for an unresolved source). For the CLEAN reconstruction (using  $\phi = D_0^{\text{clean}}$ ) this corresponds to

$T_B = (3.4 \pm 0.3) \times 10^{11}$  K. A more realistic value can be obtained instead by plugging in  $\phi = D_{\text{lim}}$ , which provides a robust lower limit of  $T_B = (1.5 \pm 0.2) \times 10^{11}$  K. Finally, for the geometrical modelling reconstruction, where no convolution takes place, setting  $\phi = D_0^{\text{chimm}}$  yields  $T_B = (8.1 \pm 0.8) \times 10^{12}$  K; this result indicates that even higher  $T_B$  are feasible for Fornax A. Overall, the magnitude of  $T_B$  suggests that the radiation is non-thermal, associated with synchrotron processes and thus likely connected to its AGN launching the jets of Fornax A.

### 3. Discussion

#### 3.1. Core structure

Given the complexity of the large scale radio lobes connected to the jet emission, it is reasonable to assume that the compact region could be fitted with a core-jet structure. In order to test this, we added a second Gaussian component to the geometrical model fit and allowed its position to vary within the entire field of view. This approach serves two purposes; firstly, it provides a constraint on the core structure. Secondly, as is the case with wide field imaging, it ensures that no other source is present in the data, thus confirming that our detection corresponds to the radio core of Fornax A. We found no significant improvement to our fiducial model of one elliptical Gaussian component. The second one is also preferably placed at the centre of the image and its corresponding flux density tends to the minimum prior value.

Finally, we examined the structure encoded in the closure phases; any discernible structure present in them is suggestive of the existence of asymmetry in the source morphology. To quantify this, we examined the mean deviation of the closure phases per triangle from zero degrees. We found that the triangle formed by CD-TD-WW exhibits a deviation of  $3.1 \sigma$  from zero degrees, by time-averaging the closure phases under a constant value assumption. In order to assess the significance of this detection, we performed a simple Monte Carlo experiment, modelling closure phases on all independent triangles as normal random variables with zero mean and standard deviation of one. We then asked how often the largest measured deviation from zero is larger than  $3.1 \sigma$ , obtaining a frequency of 8.3% as a result. Thus, we conclude with 91.7% confidence, that the CD-TD-WW triangle closure phase deviates from zero, and hence a faint source structure on scales  $\sim 4000 \mu\text{as}$ , probed by that triangle, is present.

#### 3.2. Polarisation

The observations discussed in this work were conducted in full Stokes. However, extracting polarisation information is challenging due to the faintness of the source, the absence of suitable calibrators, and due to the heterogeneous nature of the array (but demonstrated to be possible, for example, in [Dodson 2008](#)). Nevertheless, a statement can be made about the presence of circular polarisation in the signal. We imaged both parallel hand polarisations in order to investigate whether or not we could detect a mismatch in their respective flux densities. A significant discrepancy would indicate the detection of a circular polarisation signature in the data ([Event Horizon Telescope Collaboration et al. 2023](#)). We found that the difference in flux density between the two parallel hands is of the order of  $\sim 4\%$ . We note, however, that this value corresponds to a very conservative upper limit, given that the  $S/N$  is not significant enough to draw a robust conclusion. Therefore, the fractional circular polarisation

( $m_{\text{circ}}$ ) of the core of Fornax A is consistent with zero, at most  $m_{\text{circ}} \leq 4\%$ .

### 4. Conclusions

In this work we presented the first detection of the radio core of Fornax A with VLBI. Our findings can be summarised as follows:

- The core of Fornax A is best approximated by an unresolved point source.
- The best-fit model is that of a circular Gaussian component with an upper limit size of  $D_0^{\text{min}} \leq 70 \mu\text{as}$  and a flux density of  $S_0 = 47.5 - 62.3$  mJy.
- We constrained  $T_B \gtrsim 10^{11}$  K, which is suggestive of non-thermal origin for the measured radiation, possibly originating from the central SMBH of Fornax A.
- While through geometrical modelling no additional flux density was recovered, information from closure phases implies the existence of a more extended structure, the size of  $\sim 4000 \mu\text{as}$ , at a confidence level of 91.7%.
- Fractional circular polarisation of the core region is consistent with zero. A conservative upper limit is of the order of  $m_{\text{circ}} \leq 4\%$ .

Our first successful detection of Fornax A serves as a proof of concept for the detectability of this source with VLBI. Future VLBI observations including more sensitive arrays like the next generation Very Large Array, Square Kilometre Array and the Atacama Large Millimeter Array will provide further insight into the compact region of Fornax A.

*Acknowledgements.* This research is supported by the European Research Council advanced grant “M2FINDERS - Mapping Magnetic Fields with Interferometry Down to Event horizons Scales” (Grant No. 101018682). The Long Baseline Array is part of the Australia Telescope National Facility (<https://ror.org/05qajvd42>) which is funded by the Australian Government for operation as a National Facility managed by CSIRO. From the 2023 July 1, operation of Warkworth was transferred from Auckland University of Technology (AUT) to Space Operations New Zealand Ltd. Hartebeesthoek is a facility of the National Research Foundation, South Africa. This research has made use of the NASA/IPAC Extragalactic Database (NED), which is operated by the Jet Propulsion Laboratory, California Institute of Technology, under contract with the National Aeronautics and Space Administration. This research has also made use of NASA’s Astrophysics Data System Bibliographic Services. Finally, this research made use of the following python packages: *numpy* ([Harris et al. 2020](#)), *scipy* ([Virtanen et al. 2020](#)), *matplotlib* ([Hunter 2007](#)), *astropy* ([Astropy Collaboration et al. 2013, 2018](#)) and *Uncertainties: a Python package for calculations with uncertainties*.

### References

- Angioni, R., Ros, E., Kadler, M., et al. 2019, *A&A*, 627, A148  
 Astropy Collaboration, Price-Whelan, A. M., Sipőcz, B. M., et al. 2018, *AJ*, 156, 123  
 Astropy Collaboration, Robitaille, T. P., Tollerud, E. J., et al. 2013, *A&A*, 558, A33  
 Baczko, A. K., Schulz, R., Kadler, M., et al. 2016, *A&A*, 593, A47  
 Benke, P., Rösch, F., Ros, E., et al. 2024, *A&A*, 681, A69  
 Boccardi, B., Krichbaum, T. P., Bach, U., et al. 2016, *A&A*, 585, A33  
 Cantiello, M., Grado, A., Blakeslee, J. P., et al. 2013, *A&A*, 552, A106  
 Chael, A. A., Johnson, M. D., Narayan, R., et al. 2016, *ApJ*, 829, 11  
 Dasyra, K. M., Paraschos, G. F., Bisbas, T. G., Combes, F., & Fernández-Ontiveros, J. A. 2022, *Nature Astronomy*, 6, 1077  
 Dodson, R. 2008, *A&A*, 480, 767  
 EHTC, Akiyama, K., Alberdi, A., et al. 2022, *ApJ*, 930, L12  
 EHTC, Akiyama, K., Alberdi, A., et al. 2019, *ApJ*, 875, L1  
 Ekers, R. D., Goss, W. M., Wellington, K. J., et al. 1983, *A&A*, 127, 361  
 Event Horizon Telescope Collaboration, Akiyama, K., Alberdi, A., et al. 2023, *ApJ*, 957, L20  
 Fabian, A. C., Sanders, J. S., Etori, S., et al. 2000, *MNRAS*, 318, L65

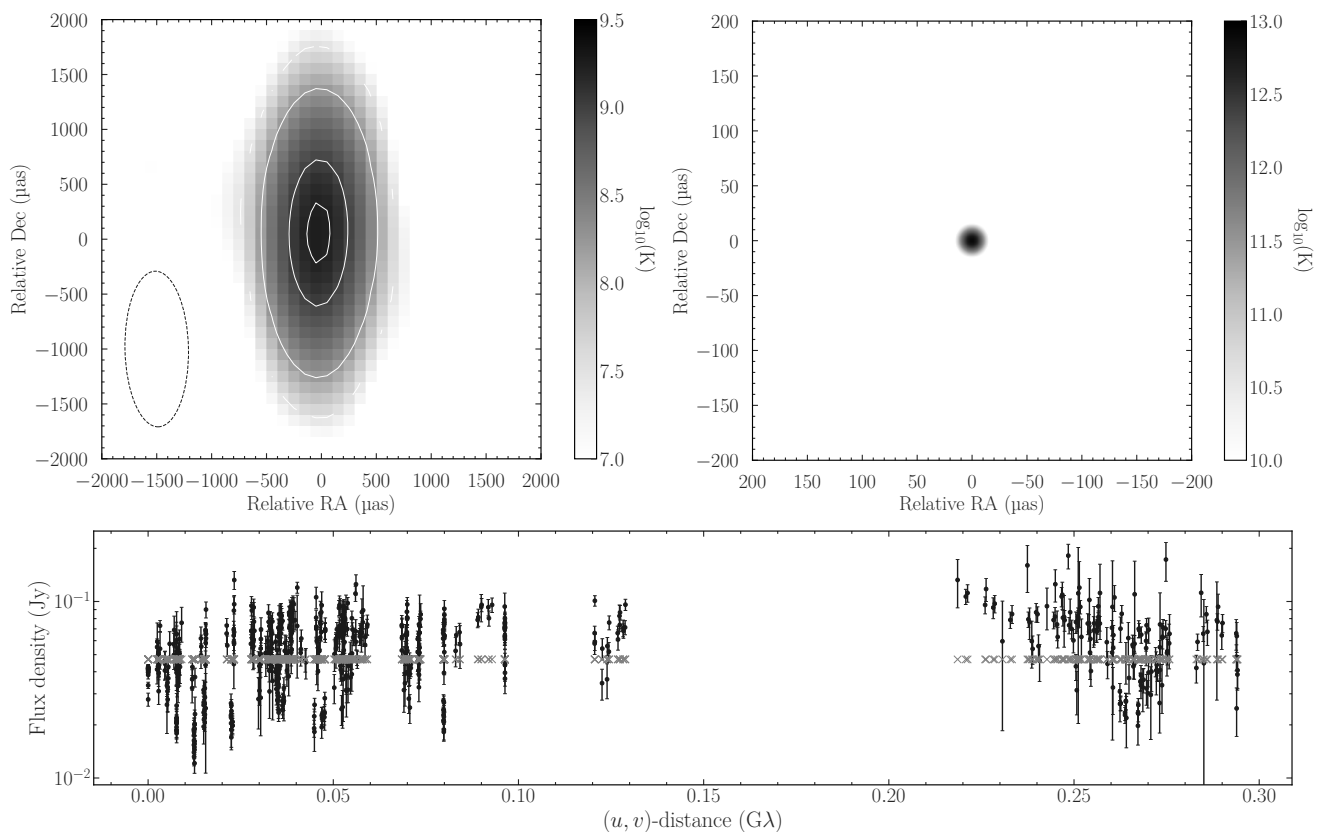


Fig. 2: Geometrical model of Fornax A using CLEAN and geometrical modelling image reconstruction and flux density versus  $(u, v)$ -distance plot. *Left*: CLEAN image of Fornax A. The structure is consistent with that of a point source, convolved with an elliptical beam of size  $580 \times 1420 \mu\text{as}$  (indicated with a dashed black ellipse in the bottom left corner). The contour levels are 1, 5, 30, 50, 75, and 95% of the intensity maximum of  $1.7 \times 10^9 \text{ K}$  and the colour scale corresponds to the measured  $T_B$ . *Right*: eht-imaging model of Fornax A. The point source structure is confirmed. The higher values recovered here stem from the fact that, in the geometrical modelling framework, beam convolution is not required and thus the small diameter of the Gaussian component plugged into Eq. 1 increases the corresponding  $T_B$ . Notice here that the axes are zoomed in by a factor of ten compared to the left panel. *Bottom*: The data and their uncertainties are shown with black dots and the best-fit model is overlaid with grey crosses. The preferred flux density level of the single Gaussian component of the model at  $S_0^{\text{ehtim}} = 47.5 \pm 4.8 \text{ mJy}$  is clearly visible.

Fomalont, E. B., Frey, S., Paragi, Z., et al. 2000, *ApJS*, 131, 95  
Fotopoulou, C. M., Dasyra, K. M., Combes, F., Salomé, P., & Papachristou, M. 2019, *A&A*, 629, A30  
García-Burillo, S., Combes, F., Usero, A., et al. 2014, *A&A*, 567, A125  
Geldzahler, B. J. & Fomalont, E. B. 1984, *AJ*, 89, 1650  
Greisen, E. W. 2003, in *Astrophysics and Space Science Library*, Vol. 285, Information Handling in Astronomy - Historical Vistas, ed. A. Heck, 109  
Harris, C. R., Millman, K. J., van der Walt, S. J., et al. 2020, *Nature*, 585, 357  
Hatt, D., Freedman, W. L., Madore, B. F., et al. 2018, *ApJ*, 866, 145  
Horellou, C., Black, J. H., van Gorkom, J. H., et al. 2001, *A&A*, 376, 837  
Hunter, J. D. 2007, *Computing in Science & Engineering*, 9, 90  
Janssen, M., Falcke, H., Kadler, M., et al. 2021, *Nature Astronomy*, 5, 1017  
Kim, J., Marrone, D. P., Roy, A. L., et al. 2018, *ApJ*, 861, 129  
Lanz, L., Jones, C., Forman, W. R., et al. 2010, *ApJ*, 721, 1702  
Lobanov, A. P. 2005, arXiv e-prints, astro  
Lu, R.-S., Asada, K., Krichbaum, T. P., et al. 2023, *Nature*, 616, 686  
Maccagni, F. M., Murgia, M., Serra, P., et al. 2020, *A&A*, 634, A9  
Mackie, G. & Fabbiano, G. 1998, *AJ*, 115, 514  
Müller, C., Kadler, M., Ojha, R., et al. 2014, *A&A*, 569, A115  
Müller, C., Kadler, M., Ojha, R., et al. 2011, *A&A*, 530, L11  
Nagai, H., Haga, T., Giovannini, G., et al. 2014, *ApJ*, 785, 53  
Nowak, N., Saglia, R. P., Thomas, J., et al. 2008, *MNRAS*, 391, 1629  
Ojha, R., Kadler, M., Böck, M., et al. 2010, *A&A*, 519, A45  
Paraschos, G. F., Kim, J. Y., Krichbaum, T. P., & Zensus, J. A. 2021, *A&A*, 650, L18  
Paraschos, G. F., Kim, J. Y., Wielgus, M., et al. 2024, *A&A*, 682, L3  
Paraschos, G. F., Krichbaum, T. P., Kim, J. Y., et al. 2022, *A&A*, 665, A1  
Richtler, T., Bassino, L. P., Dirsch, B., & Kumar, B. 2012a, *A&A*, 543, A131  
Richtler, T., Kumar, B., Bassino, L. P., Dirsch, B., & Romanowsky, A. J. 2012b, *A&A*, 543, L7

Roelofs, F., Johnson, M. D., Chael, A., et al. 2023, *ApJ*, 957, L21  
Schweizer, F. 1980, *ApJ*, 237, 303  
Shepherd, M. C., Pearson, T. J., & Taylor, G. B. 1994, in *Bulletin of the American Astronomical Society*, Vol. 26, 987–989  
Slee, O. B., White, G. L., Reynolds, J. E., & Caganoff, S. 1990, *Astrophysical Letters and Communications*, 27, 361  
Stanley, G. J. & Slee, O. B. 1950, *Australian Journal of Scientific Research A Physical Sciences*, 3, 234  
Virtanen, P., Gommers, R., Oliphant, T. E., et al. 2020, *Nature Methods*, 17, 261